Low-loss wavelength-multiplexed optical scanners using volume Bragg gratings for transmit-receive lasercom systems

Zahid Yaqoob, MEMBER SPIE
Nabeel A. Riza, FELLOW SPIE
University of Central Florida
School of Optics
Center for Research and Education in Optics and Lasers
Photonic Information Processing Systems Laboratory
4000 Central Florida Boulevard
Orlando, Florida 32816-2700
E-mail: nriza@mail.ucf.edu

Abstract. Low-loss, no moving parts, free-space wavelength-multiplexed optical scanner (W-MOS) modules for transmit-receive lasercom systems are proposed and experimentally demonstrated. The proposed scanners are realized using volume Bragg gratings stored in dichromated gelatin (DCG) coupled with high-speed wavelength selection, such as by a fast tunable laser. The potential speed of these scanners is in the gigahertz range using present-day state of the art nanosecond tuning speed lasers. A 940-lines/mm volume Bragg grating stored in dichromated gelatin is used to demonstrate the scanners. Angular dispersion and diffraction efficiency of the volume Bragg grating used for demonstration are studied, versus wavelength and angle of incidence to determine the free-space W-MOS angular scan and insertion loss, respectively. Experimental results show that a tunable bandwidth of 80 nm, centered at 1560 nm, delivers an angular scan of 6.25 deg. The study also indicates that an in-line scanner design realized using two similar Bragg gratings in DCG delivers a 13.42-deg angular scan, which is more than double the angular scan available from the free-space W-MOS using a single volume Bragg grating. Furthermore, a free-space W-MOS using a single Dickson grating features low ($<$0.15 dB) polarization-dependent loss and an average scanner insertion loss of only 0.4 dB over the 70-nm wavelength band around 1550 nm. [DOI: 10.1117/1.1690765]

Subject terms: optical scanners; free-space lasercom; Bragg diffraction gratings; wavelength multiplexing.

Paper 030430 received Sep. 2, 2003; revised manuscript received Oct. 31, 2003; accepted for publication Nov. 26, 2003. This paper is a revision of a paper presented at the SPIE conference on Free-Space Laser Communication and Active Laser Illumination III, Aug. 2003, San Diego, CA. The paper presented there appears (unrefereed) in SPIE Proceedings Vol. 5160.

1 Introduction

Free-space optical communication systems due to their large information capacity are emerging as an attractive choice for alleviating data communication bottlenecks at different levels of the information highway.[1,2] The narrow beam width of the laser is one of the major advantages of free-space optical communications, as it allows sending information with high directivity (low side lobes) and security, which in turn makes the system efficient in power consumption. The high directivity of a laser beam, however, brings forward serious challenges related to beam-pointing technology in free-space optical communication systems. The problem is compounded by the fact that the amplitude of vibrations in moving platforms is much bigger than the laser beam size.[3] Thus, beam pointing and tracking control systems with fast and agile fine beam pointing (e.g., ± 5 μrad)[4] capabilities need to be an integral part of a lasercom subsystem to reduce moving platform vibration errors for reduced data bit error rates. Specifically, there is a need to realize a large aperture (e.g., 10 cm diam) scanner that also has low power consumption (e.g., milliwatts) and is rapidly (e.g., a few microseconds) reconfigurable. Hence, there exists a size versus speed dilemma if moving-parts optics is deployed for beam pointing. We present scanners using volume Bragg gratings stored in dichromated gelatin that promise low-loss, high-speed, and high resolution 1-D wide angular scans.

In the 1970s, it was realized that laser wavelength changes, combined with wavelength sensitive optics, could be used for laser beam steering.[5,6] Independently, we have proposed, analyzed, and demonstrated how extremely fast wavelength selection, combined with present day planar dispersive elements (e.g., diffraction gratings), can be used to realize a 1-D beam scanner, known as the free-space wavelength-multiplexed optical scanner (W-MOS).[7] Free-space W-MOS simultaneously provides fast speed, large apertures, subdegree scan resolution, 1-D wide angular scans, and simple control. Experimental demonstration of a free-space W-MOS using blazed reflection grating (600 lines/mm) shows high resolution ($\leqslant$1-mrad beam divergence for a 1.875-cm diffraction-limited aperture diameter) and large angular scans ($\sim$13 deg).[8] The study indicates that choosing a suitable angle of incidence on the diffraction grating can increase the angular scan range of the scan-

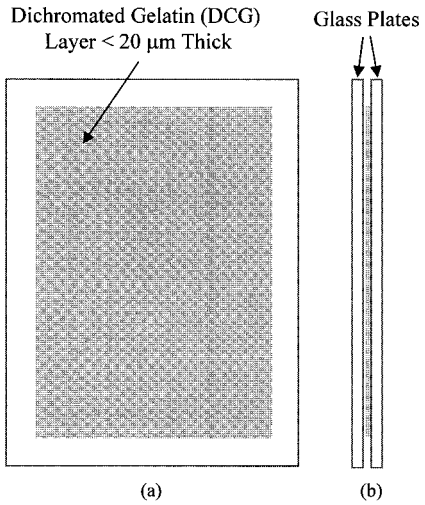

Fig. 1 Schematic of a volume Bragg grating in dichromated gelatin: (a) front view and (b) side view.

ner. However, failing to satisfy the Littrow configuration significantly degrades the diffraction efficiency of a blazed grating versus wavelength, causing higher scanner insertion loss. Because transmissive surface relief sinusoidal phase gratings cannot deliver high diffraction efficiency in the infrared region (1550 nm), the alternative would be to use volume Bragg gratings that guarantee clear scanner aperture as well as symmetric design for effective scanner operation. Recently, we proposed and showed, to our knowledge for the first time, how robust, high-efficiency narrowband tilted volume Bragg gratings in photothermorefractive glass,[9,10] combined with high-speed wavelength selection, can be used to realize a desired fast-beam-switching, large-aperture, 2-D scanner.[11] In this work,[12] we present and discuss in detail the functionality of volume Bragg gratings stored in dichromated gelatin, also known as Dickson gratings,[13] for use in free-space W-MOS, capable of 1-D beam scanning. Grating design parameters such as loss and diffraction efficiency versus wavelength is discussed. Based on diffraction efficiency measurements, grating structure thickness and the index of modulation are estimated. Dickson grating-based free-space W-MOS modules are presented, and scanner parameters such as insertion loss and angular scan versus wavelength of the tunable source are discussed.

2 Volume Phase Gratings in Dichromated Gelatin

Volume phase gratings recorded interferometrically in dichromated gelatin (DCG), also known as Dickson gratings, offer a very high index of modulation that makes it possible to record volume phase gratings with very small thickness ($<20\ \mu$m), yet can still offer extremely high diffraction efficiency (>95%). Furthermore, the small thickness of the volume phase gratings in Dickson gratings makes them less selective in λ, i.e., almost flat response over the desired wavelength band. The construction of a Dickson grating is shown in Fig. 1. A thin layer of DCG ($<20\ \mu$m thick) is deposited on a glass plate [see the glass plate on the right-hand side in Fig. 1(b)]. When the volume phase grating is recorded and fixed, matching index glue is applied on the DCG layer before a second glass plate [shown on the left-hand side in Fig. 1(b)] is placed on it and sealed with a telecom-grade epoxy. Since the bulk index of refraction of DCG is 1.3 and there is no index matching glue between one of the two DCG-glass interfaces, Fresnel reflection loss in the range of 0.04 to 0.14 dB is observed, depending on the index of the glass plate between 1.50 and 1.70. The volume phase grating designed for telecom has 940-lines/mm spatial frequency, which corresponds to a grating period $L=1.0638\,\mu$m. At Bragg wavelength $\lambda_B=1550$ nm, the Bragg angle in air is $\theta_{B,\mathrm{air}}=46.76$ deg.

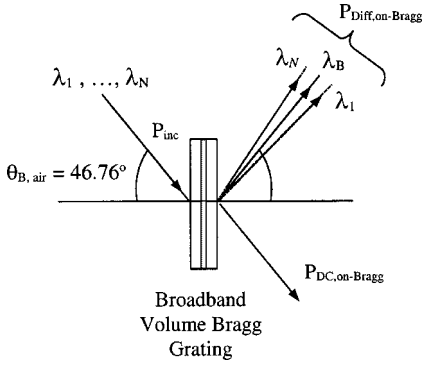

Fig. 2 Experimental setup to study loss as well as relative and absolute diffraction efficiencies of a Dickson grating; $\lambda_B=1550$ nm.

To study the diffraction efficiency of a Dickson grating, a collimated beam from a broadband source with $1/e^2$ beam size of ~1 mm is incident on the grating mounted on a rotational stage to adjust the angle of incidence (see Fig. 2). The angle of incidence is set to $\theta_{\mathrm{inc}}=\theta_{B,\mathrm{air}}=46.76$ deg to satisfy the Bragg condition at $\lambda_B=1550$ nm. An optical spectrum analyzer is used to measure the optical power in the incident and undiffracted (zero-order) beams to determine loss (due to absorption or scattering), and the optical power diffracted into the first order to estimate the absolute as well as relative diffraction efficiencies of the Dickson grating versus wavelength.

Figures 3(a) through 3(d) show the static loss, relative diffraction efficiency, absolute diffraction efficiency, and polarization dependent loss (PDL), respectively, of the Dickson grating versus wavelength of the broadband source in a 70-nm band around $\lambda_B=1550$ nm. The study shows that the static loss (dB) varies from 0.4 to 0.25 dB as the wavelength is changed from 1520 to 1590 nm. The average static loss over the 70-nm tunable band is $\sim 0.3\pm 0.05$ dB. The maximum value of the relative diffraction efficiency, which is defined as the ratio of $P_{\mathrm{Diff,on\text{-}Bragg}}$ to $P_{\mathrm{DC,off\text{-}Bragg}}$, is measured as 99.75 ± 0.05 %, where $P_{\mathrm{Diff,on\text{-}Bragg}}$ is the optical power in the first-order diffracted beam at Bragg ($\lambda_B=1550$ nm), and $P_{\mathrm{DC,off\text{-}Bragg}}$ is the optical power in the undiffracted DC beam when the Bragg condition is not satisfied ($\theta_{\mathrm{inc,air}}\neq\theta_{B,\mathrm{air}}$). Figure 3(b) shows that the relative diffraction efficiency does not drop sharply with the wavelength and is symmetric about $\lambda_B=1550$ nm. Similarly, the study of the absolute diffraction efficiency, defined as the ratio of $P_{\mathrm{Diff,on\text{-}Bragg}}$ to P_{inc}, shows that the maximum absolute diffraction efficiency is ~93.0%, where P_{inc} is the

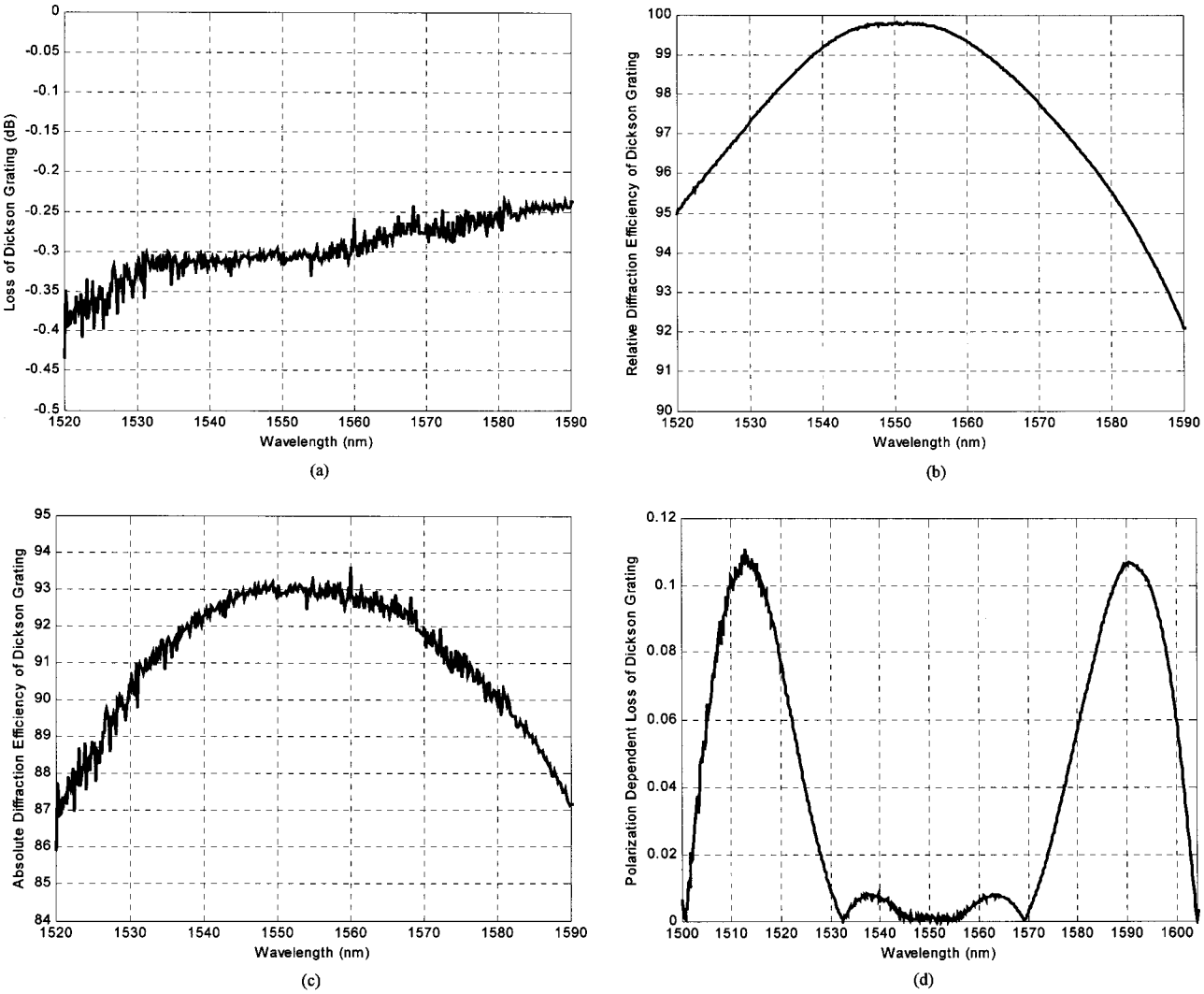

Fig. 3 Measured (a) loss, (b) relative diffraction efficiency, (c) absolute diffraction efficiency, and (d) polarization dependent loss of the Dickson grating versus wavelength; $\lambda_B = 1550$ nm.

optical power in the incident beam [see Fig. 3(c)]. Note that the absolute diffraction efficiency is not symmetric about $\lambda_B = 1550$ nm because the loss (dB) is not uniform over the wavelength band under consideration. The experimental study also indicates that the absolute diffraction efficiency remains >87% over the 70-nm wavelength band. The PDL of the grating is defined as $10 \times \log(P_{\max}/P_{\min})$, where $P_{\max}$ and $P_{\min}$ are the maximum and minimum optical powers, respectively, in the diffracted beam as the polarization of the incident light is changed. Figure 3(d) shows the measured PDL of the grating versus wavelength of the source. As expected, the measured PDL is minimum at the Bragg wavelength $\lambda_B = 1550$ nm. However, the PDL increases and drops down again as the wavelength is changed. Furthermore, the measured PDL is symmetric about the Bragg wavelength. The plot indicates that the PDL remains less than 0.15 dB over a significant band around 1550 nm.

To estimate the thickness d of the DCG layer and the index of modulation Δn of the recorded phase grating, the dephasing parameter ξ in the expression for diffraction efficiency η given by[14]

$$\eta = \frac{\gamma^2}{\gamma^2 + \xi^2} \sin^2[\sqrt{\gamma^2 + \xi^2}] \tag{1}$$

is determined for a known value of η at an off-Bragg wavelength $\lambda = \lambda_B + \Delta\lambda$. Note that γ is the coupling parameter given by[14]

$$\gamma(\lambda) = \frac{\pi \Delta n d}{\lambda \cos \theta_{\text{inc},g}}, \tag{2}$$

where $\theta_{\text{inc},g}$ is the angle of incidence inside the DCG layer. Since the maximum relative diffraction efficiency $\eta_B = 0.9975$ [see Fig. 3(b)], the corresponding value of the coupling parameter comes out to be $\gamma_B = 1.5208$. The thickness d of the DCG is estimated in an iterative fashion as follows. First of all, the preliminary value of dephasing

parameter ξ is calculated from Eq. (1) as 0.349 (assuming initially $\gamma = \gamma_B$ at $\lambda_1 = 1520$ nm for the first iteration). Next, the thickness d of the DCG is estimated from the following relation[14]

$$\frac{\Delta\lambda}{\lambda_B} = -\frac{\xi L}{\pi d \tan\theta_{\mathrm{inc},g}}, \tag{3}$$

where $\Delta\lambda = -30$ nm, $L = 1.0638\,\mu$m, and $\theta_{\mathrm{inc},g} = 35.969$ deg. The estimated value of thickness d of the DCG layer comes out to be 8.25 μm. The estimated value of d is then used to determine the index of modulation Δn using Eq. (2). By substituting the values of $\gamma_B = 1.5208$, $\lambda_B = 1550$ nm, $\theta_{\mathrm{inc},g} = 35.97$ deg, and $d = 8.25\,\mu$m in Eq. (2), the index of modulation is estimated as $\Delta n = 73.6 \times 10^{-3}$. Next, the value of γ is determined at $\lambda = 1520$ nm using the same relation [Eq. (2)]. Iteratively, the new value of γ is used to estimate again values of ξ, d, Δn, and γ. Note that the procedure converges very fast (e.g., in two to three iterations). The final values of d and Δn are estimated as 8.39 ± 0.05 μm and $(72.4 \pm 0.2) \times 10^{-3}$, respectively. Note that this estimated value of Δn is almost 72 times the maximum index of modulation possible in photothermorefractive glass.

3 Free-Space Wavelength-Multiplexed Optical Scanner Using Dickson Gratings

As discussed in the earlier section, owing to the very high index of modulation ($\sim 72.4 \times 10^{-3}$) possible in dichromated gelatin (DCG), volume phase gratings with extremely high diffraction efficiency (>95%) can be recorded in very small thicknesses of the DCG layer. Furthermore, the small thickness of the DCG layer in Dickson gratings makes them less selective in wavelength. Hence, the two properties, i.e., high diffraction efficiency and low wavelength selectivity, make Dickson gratings suitable for applications like free-space W-MOS requiring low-loss broadband operations. The scanner insertion loss of free-space W-MOS, defined as $10 \times \log(\eta_{\mathrm{abs}})$, where η_{abs} is the absolute diffraction efficiency [already discussed and shown in Fig. 3(c)], is shown in Fig. 4. The minimum value of scanner insertion loss is 0.315 at $\lambda_B = 1550$ nm. The average scanner insertion loss over the 70-nm tunable band is 0.4 dB. Because there is at least one dichromated gelatin layer-glass interface that has an index mismatch, Fresnel reflection loss in the range 0.04 to 0.14 dB is expected for glass plate index of refraction in the range 1.5 to 1.7, respectively.

To study the angular scan available from the free-space W-MOS using volume Bragg grating in dichromated gelatin, a setup similar to that shown in Fig. 2. was built in the laboratory. A collimated beam from a fiber-coupled tunable laser source (with $1/e^2$ beam size of ~ 0.6 mm) is incident on the grating mounted on a rotational stage to adjust the angle of incidence (see Fig. 2). The Bragg angle is set to $\theta_{B,\mathrm{air}} = 46.76$ deg to satisfy the Bragg condition at $\lambda_B = 1550$ nm. An infrared camera is used to observe the scanning first diffraction order when the wavelength of the tunable laser is tuned over the 80-nm wavelength band centered at 1560 nm. The angular deflection is measured by tracking the scanning first diffraction order with the help of an iris mounted on an aluminum C-channel, with one end attached to a rotational stage having the same axis of rotation as that for the Bragg grating. A total angular scan of 6.25 deg was measured by tuning the wavelength of the source from 1520 to 1600 nm. Furthermore, the angular scan available over the 80-nm tunable band is estimated using the grating equation[15]

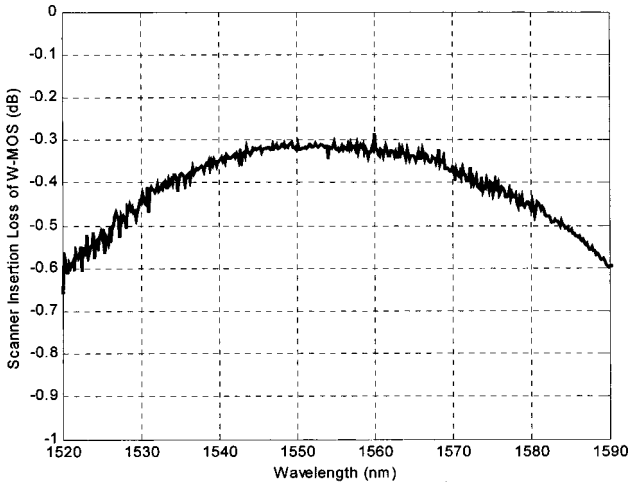

Fig. 4 Scanner insertion loss of free-space wavelength-multiplexed optical scanner versus wavelength; $\lambda_B = 1550$ nm.

$$\theta_{\mathrm{out,air}} = \sin^{-1}\left\{\frac{\lambda}{L} - \sin\theta_{\mathrm{inc,air}}\right\}. \tag{4}$$

Figure 5 shows both experimental and theoretical angular scans (in degrees) versus the wavelength of the tunable source. The plot indicates that the measured angular scan is almost consistent with the estimated scan of 6.39 deg as the source is tuned over the 80-nm tunable bandwidth around 1560 nm.

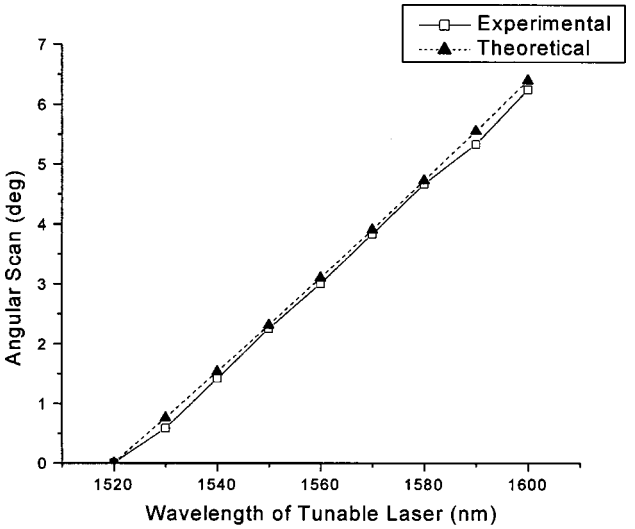

Fig. 5 Angular scan available from a free-space W-MOS using a single Dickson grating versus wavelength.

Equation (4) suggests that an angular scan of 9.48 deg is possible if the wavelength of the source is tuned over a 120-nm bandwidth centered at $\lambda_B = 1550$ nm ($\theta_{\text{inc}} = \theta_{B,1550} = 46.76$ deg). However, the measured relative diffraction efficiency of the Dickson grating (Bragg set at 1550 nm) drops to ~80% around the edges of the tunable band [see Fig. 6(a)]. It is important to note that angular scans of 4.53 and 4.95 deg are possible when the grating is Bragg set at $\lambda_B = 1520$ nm ($\theta_{\text{inc}} = \theta_{B,1520} = 45.59$ deg) and 1580 nm ($\theta_{\text{inc}} = \theta_{B,1580} = 47.95$ deg), and the wavelength of the source is tuned from $\lambda = 1475$ to 1535 nm and 1565 to 1625 nm, respectively. Moreover, the sum of the two tunable bands and the angular scan ranges are 120 nm and 9.48 deg, respectively (same as in the previous case). The relative diffraction efficiency of the Dickson grating for the two cases, i.e., $\lambda_B = 1520$ nm ($\theta_{\text{inc}} = 45.59$ deg) and 1580 nm ($\theta_{\text{inc}} = 47.95$ deg) was also measured versus wavelength, and the results are shown in Figs. 6(b) and 6(c). The two plots clearly indicate that the overall relative diffraction efficiency of the Dickson grating is better than the case when the grating is Bragg set at $\lambda_B = 1550$ nm and the wavelength of the source is tuned over 120 nm [see Fig. 6(a)]. It can therefore be concluded that it is better to choose smaller distributed tunable bands rather than a single large tunable band to achieve overall higher diffraction efficiency, which indicates lower average scanner insertion loss but still the same angular scan range. However, we will be required to efficiently adjust the appropriate angle of incidence for each corresponding tunable band.

Figure 7 shows the schematic of a free-space W-MOS that uses a fast (microsecond speed) 1×2 fiber-coupled broadband optical switch to adjust the angle of incidence on the Dickson grating. The two output fibers of the optical switch end up in an assembly that keeps the polished ends of the single-mode fibers (SMFs) one focal length distance from an achromatic lens. The two SMFs are parallel with each other, such that one of the fibers is aligned with the principal axis of the lens, whereas the other is shifted by x' (see Fig. 7). The elevation angles and $1/e^2$ beam diameter (BD) of the collimated beams after the lens are given by

$$\theta' = -\tan^{-1}\left(\frac{x'}{f}\right), \tag{5}$$

and

$$1/e^2\text{BD} = \frac{2\lambda f \cos\theta'}{\pi w_{\text{inc}}}, \tag{6}$$

respectively, where f is focal length of the collimating lens and w_{inc} is the beam waist (half of the mode field diameter) of the Gaussian beam coming out of the SMFs. For instance, using $f = 75$-mm focal length lens, $x' = 3.09$ mm will yield $\theta' = 2.359$ deg (the difference in Bragg angles for $\lambda_B = 1520$ and 1580 nm). Therefore, a collimated beam from port 2 of the optical switch will be incident on the Dickson grating at $\theta_{\text{inc}} = 47.953$ deg (the Bragg angle for $\lambda_B = 1580$ nm), whereas the collimated beam from port 1 of the optical switch will be incident on the Dickson grating at $\theta_{\text{inc}} = 45.594$ deg (the Bragg angle for $\lambda_B = 1520$ nm).

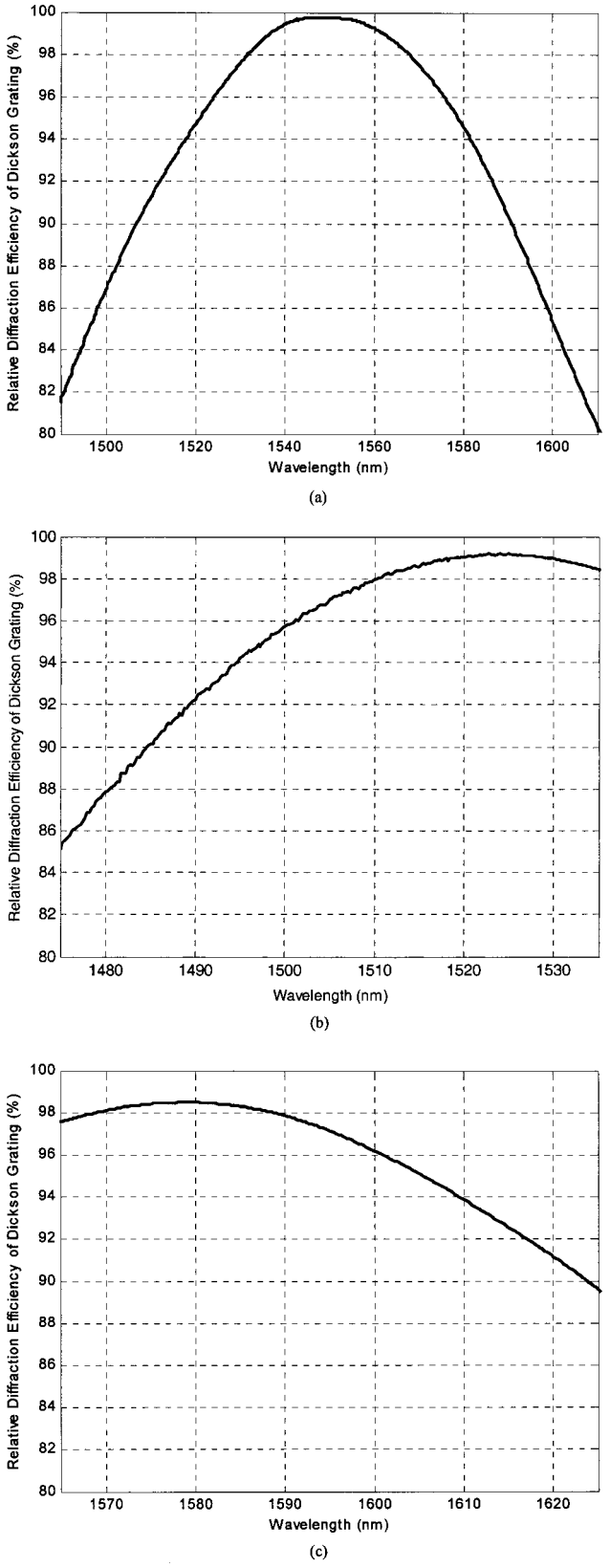

Fig. 6 Relative diffraction efficiency of Dickson grating for (a) $\lambda_B = 1550$ nm, $\theta_{\text{inc}} = 46.76$ deg, $\lambda = 1490$ to 1610 nm; (b) $\lambda_B = 1520$ nm, $\theta_{\text{inc}} = 45.59$ deg, $\lambda = 1475$ to 1535 nm; and (c) $\lambda_B = 1580$ nm, $\theta_{\text{inc}} = 47.95$ deg, $\lambda = 1565$ to 1625 nm.

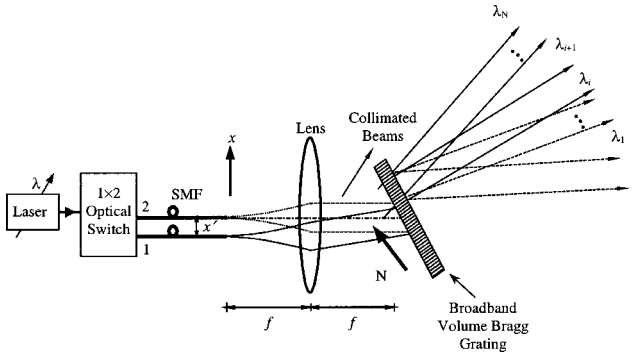

Fig. 7 Schematic of a smart free-space W-MOS with incidence angle setting capability for very high overall throughput. *N* is the grating normal; SMF is the single mode fiber; and *f* is the focal length of the collimating lens.

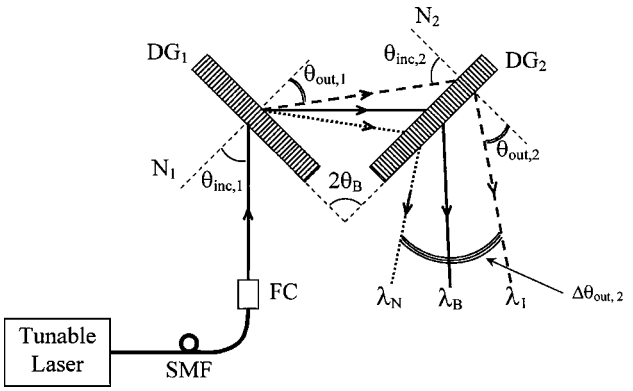

Fig. 8 Two similar Dickson gratings arranged in a symmetrical fashion (such that the angle between the planes of the two gratings is $2\theta_B$) for wide total angular scan range. N_i is normal to the i'th grating; DG_i is the i'th Dickson grating; SMF is the single mode fiber; and FC is the fiber collimator (such as a gradient index lens).

Hence, from an operational point of view, the optical switch will be set to route the input light to port 1 (that will set $\theta_{\text{inc}}=45.594$ deg on the grating), and the wavelength of the laser will be tuned from 1475 to 1535 nm. This will cause the diffracted beam to go through an angular displacement from 42.23 to 46.76 deg. Next, the optical switch will be set to route the input light to port 2 (that will set $\theta_{\text{inc}}=47.953$ deg), and the wavelength of the laser will be tuned from 1565 to 1625 nm to get the rest of the angular scan from 46.76 to 51.71 deg with high overall throughput. Note that the two angular scan regions do not have a discontinuity, as the second scan starts from the angular position where the first scan ends. Furthermore, the sum of the individual angular scan ranges corresponding to the distributed wavelength tunable band (60 nm each) is also equal to the angular scan that would be available if the grating was Bragg set at 1550 nm and a single 120-nm tunable band was used. Moreover, the idea can be extended by increasing the number of output ports of the optical switch (such as three or more).

4 In-Line Design of a Free-Space Wavelength-Multiplexed Optical Scanner with Wide Angular Scan Range

As discussed earlier, because of the high spatial frequency (940 lines/mm) in Dickson gratings, the Bragg angle is significantly large ($\theta_B=46.76$ deg at $\lambda_B=1550$ nm), which makes the first-order beam diffract almost in an orthogonal direction to the incident beam. A total angular scan of 6.25 deg has also been demonstrated by tuning the wavelength of the incident beam from 1520 to 1600 nm. At this point, the motivation is to design an inline free-space W-MOS that can also deliver increased total angular scan range (using the same tunable bandwidth of the laser source). Figure 8 shows two similar Dickson gratings arranged in a symmetrical fashion, such that the angle between the planes of the two gratings is $2\theta_B$, where θ_B is the Bragg incidence angle corresponding to the Bragg wavelength λ_B. Because $\theta_{\text{inc},1}=\theta_B$, the Bragg wavelength diffracts out at θ_B from the first grating and sets an angle of incidence $\theta_{\text{inc},2}=\theta_B$ at the second grating, which causes it to diffract again at θ_B (see Fig. 8).

As the wavelength of the laser source is tuned around the Bragg wavelength λ_B, the angular scan after the first grating will be given by

$$\theta_{\text{out},1}=\sin^{-1}\left\{\frac{\lambda}{L}-\sin\theta_B\right\}. \tag{7}$$

The scanning beam from the first Dickson grating will be incident on the second Dickson grating at an angle given by

$$\theta_{\text{inc},2}=2\theta_B-\theta_{\text{out},1}, \tag{8}$$

where $\theta_{\text{out},1}$ is given by Eq. (7). Hence, the final angular scan after the second Dickson grating (DG) will be

$$\theta_{\text{out},2}=\sin^{-1}\left\{\frac{\lambda}{L}-\sin\theta_{\text{inc},2}\right\}$$
$$=\sin^{-1}\left\{\frac{\lambda}{L}-\sin\left[2\theta_B-\sin^{-1}\left(\frac{\lambda}{L}-\sin\theta_B\right)\right]\right\}. \tag{9}$$

Note that all the angles in Eqs. (7) to (9) are measured with respect to the grating normals N_1 and N_2. Thus the angular scan after DG_1 and DG_2 will be

$$\Delta\theta_{\text{out},1}=\sin^{-1}\left\{\frac{\lambda_N}{L}-\sin\theta_B\right\}-\sin^{-1}\left\{\frac{\lambda_1}{L}-\sin\theta_B\right\}, \tag{10}$$

and

$$\Delta\theta_{\text{out},2}=\sin^{-1}\left\{\frac{\lambda_N}{L}-\sin\left[\sin^{-1}\left(\frac{\lambda_N}{L}-\sin\theta_B\right)\right]\right\}$$
$$-\sin^{-1}\left\{\frac{\lambda_1}{L}-\sin\left[\sin^{-1}\left(\frac{\lambda_1}{L}-\sin\theta_B\right)\right]\right\}, \tag{11}$$

respectively. Finally, the setup in Fig. 8 is improved by adding two infrared mirrors for optical path folding to realize an in-line free-space W-MOS (see Fig. 9). Because the incident beam is horizontal, the Bragg wavelength λ_B diffracts out from DG_1 at θ_B. The mirror M_1 is oriented such

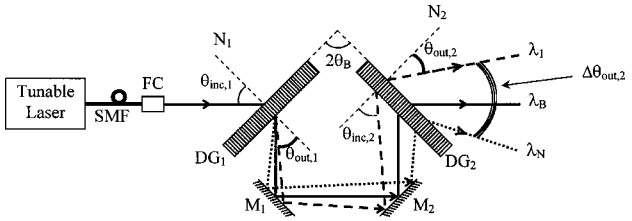

Fig. 9 Schematic of an in-line wide angle free-space W-MOS using two Dickson gratings and two mirrors (for optical path folding). N_i is normal to the i'th grating; DG_i is the i'th Dickson grating; M_i is the i'th mirror; SMF is the single mode fiber; and FC is the fiber collimator.

that it makes an angle $-\theta_B$ with the horizontal. The wavelength λ_B will therefore reflect from M_1 to become horizontal again. The mirror M_2 is vertically symmetric to M_1, i.e., it makes an angle θ_B with the horizontal, which causes λ_B to reach DG_2 at $\theta_{\text{inc},2}=\theta_B$. Thus, the Bragg wavelength λ_B diffracts from DG_2 to come out horizontal. The analysis for angular deflection and total angular scan range as a function of wavelength (given before for the setup in Fig. 8) also holds for the one shown in Fig. 9, since both the setups are equivalent. Furthermore, Dickson gratings are transmissive volume Bragg gratings, where the incident and diffracted beams are symmetric to the grating plane at the Bragg wavelength. This indicates that a free-space W-MOS design using n gratings ($n=1,2$) will have a scanner aperture d_{out} given by

$$d_{\text{out}}=2w_{\text{inc}}\cos(\theta_{\text{out},n}-\theta_B), \tag{12}$$

where w_{inc} is the beam waist of the incident Gaussian beam and $\theta_{\text{out},n}$; $n=1$, 2, is the output scan angle. It can therefore be concluded that although the scanner aperture will vary with the output scan angle, it will remain approximately the size of the incident beam, since $\cos(\theta_{\text{out},n}-\theta_B)$ will be ~ 1.

To study the angular scan available from the setup in Fig. 8 (or Fig. 9), a proof-of-concept experimental setup (shown in Fig. 10) is built in the laboratory. The experimental setup uses a Dickson grating and a mirror to simulate two Dickson gratings arranged symmetrically (in Fig. 8). A collimated beam from a fiber-coupled tunable laser (with $1/e^2$ beam size of ~ 0.6 mm) is incident on the grating mounted on a rotational stage to adjust the angle of incidence. The angle of incidence is set to $\theta_{\text{inc},1}=\theta_B=46.76$ deg to satisfy the Bragg condition at $\lambda_B=1550$ nm. An infrared mirror is placed close to the Dickson grating, such that the diffracted beam at $\lambda=\lambda_B=1550$ nm ray traces its own path, diffracts again, and reaches the fiber collimator. An infrared camera is used to observe the scanning double-diffracted beam, as the wavelength of the tunable laser is tuned over the 80-nm wavelength band centered at 1560 nm. The angular deflection is measured by tracking the scanning beam with the help of an iris mounted on an aluminum C-channel, with one end attached to a rotational stage having the same axis of rotation as that for the Bragg grating. A total angular scan of 13.42 deg is measured using the setup in Fig. 10, as the wavelength of the source is changed from 1520 to 1600 nm. It is important to notice that the measured scan is in complete agreement with the theoretical angular scan of 13.39 deg estimated by Eq. (11) for the same 80-nm tunable bandwidth.

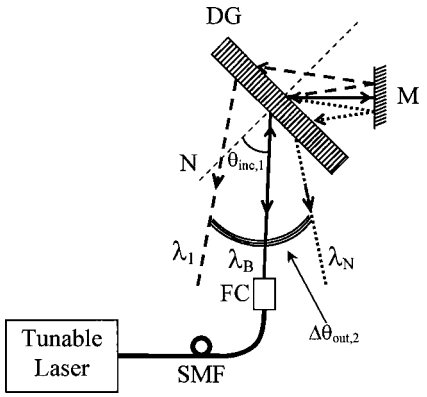

Fig. 10 Experimental setup to simulate the in-line wide angle free-space W-MOS in Fig. 9 and study the angular scan range.

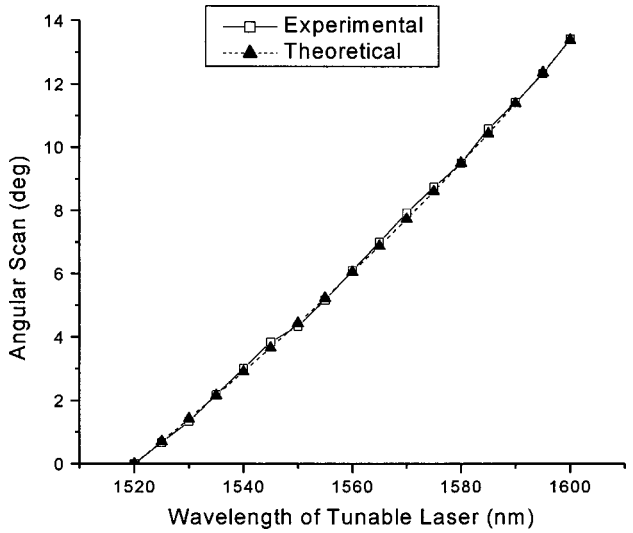

Fig. 11 Free-space W-MOS angular scan (for two Dickson gratings) versus wavelength of the tunable source.

Recall that the angular scan range available from the free-space W-MOS using a single Dickson grating is only 6.39 deg. It is therefore obvious that the angular scan range for an in-line W-MOS (using two Dickson gratings) is more than double the scan range that is available from the W-MOS design using a single Dickson grating. Figure 11 shows both experimental and theoretical angular scans (in degrees) versus wavelength of the tunable source.

5 Conclusion

In conclusion, a very high index of modulation is possible in dichromated gelatin that allows designing volume phase gratings (known as Dickson gratings) with very small thicknesses (<10 μm), yet very high diffraction efficiency ($>95\%$). The small thickness of the dichromated gelatin layer in Dickson gratings makes them less selective in wavelength. The two characteristics, i.e., high diffraction

efficiency and low wavelength selectivity of Dickson gratings, make them suitable for use in the free-space W-MOS. Also, high spatial frequency (940 lines/mm) provides significant dispersion (6.25-deg angular scan measured over a 80-nm bandwidth around 1560 nm). An in-line double-scan range free-space W-MOS design for enhanced scanner operations is also discussed that uses two Dickson gratings and two mirrors for optical path folding. Experimental study (using a setup that simulates the dispersive capabilities of an in-line W-MOS) indicates that a total angular scan of 13.42 deg is obtained when the laser source is tuned over a 80-nm bandwidth around 1560 nm. In addition, a free-space W-MOS using a single Dickson grating features low ($<$0.15 dB) polarization-dependent loss and an average scanner insertion loss of only 0.4 dB over the 70-nm wavelength band around 1550 nm. Furthermore, Dickson gratings are transmissive volume Bragg gratings, where the incident and diffracted beams are symmetric to the grating plane at the Bragg wavelength. This indicates that a free-space W-MOS design using such gratings will have a scanner aperture approximately the size of the incident beam. Using fast tunable lasers or optical filters coupled with a broadband source, the proposed free-space W-MOS features microsecond domain scan setting speeds, low scanner insertion loss, and single/multiple beam(s) in space. Because Dickson gratings are holographic phase gratings stored in dichromated gelatin layer sandwiched between glass plates, very large (e.g., several centimeters or more) diameter free-space W-MOS scanner apertures are possible for subdegree angular scans. The potential speed of this scanner is in the gigahertz range using present-day state of the art nanosecond tuning speed lasers.[16,17] Future work relates to the demonstration of the in-line free-space W-MOS with wide angular scan range capabilities.

Acknowledgment

This work is partially supported by DARPA grant N66001-98-D-6003.

References

1. P. J. Winzer and W. R. Leeb, ''Space-borne optical communications—A challenging reality,'' Special Symp. on Agile Optical Beams and Applications, IEEE LEOS 15th Annual Meeting, Nov. 10–14, 2002, Glasgow, Scotland, Invited Paper (WD2).
2. G. S. Mecherle, ''Active pointing for terrestrial free space optics,'' Special Symp. on Agile Optical Beams and Applications, IEEE LEOS 15th Annual Meeting, Nov. 10–14, 2002, Glasgow, Scotland, Invited Paper (WL1).
3. C. Chen, J. W. Alexender, H. Hemati, S. Monacos, T. Yan, S. Lee, J. R. Lesh, and S. Zingales, ''System requirements for a deep space optical transceiver,'' *Proc. SPIE* **3615**, 142–152 (1999).
4. W. Klaus, ''Development of LC optics for free-space laser communications,'' *Int. J. Electron. Commun.* **56**(4), 243–253 (2002).
5. R. L. Forward, ''Passive beam-deflecting apparatus,'' U.S. Patent No. 3,612,659 (1971).
6. K. G. Leib, ''Radiation beam deflection system,'' U.S. Patent No. 4,250,465 (1981).
7. Z. Yaqoob, A. A. Rizvi, and N. A. Riza, ''Free-space wavelength-multiplexed optical scanner,'' *Appl. Opt.* **40**(35), 6425–6438 (2001).
8. Z. Yaqoob and N. A. Riza, ''Free-space wavelength-multiplexed optical scanner demonstration,'' *Appl. Opt.* **41**(26), 5568–5573 (2002).
9. L. B. Glebov, N. V. Nikonorov, E. I. Panysheva, G. T. Petrovskii, V. V. Savvin, I. V. Tunimanova, and V. A. Tsek-homskii, ''New ways to use photosensitive glasses for recording volume phase holograms,'' *Opt. Spectrosc.* **73**, 237–241 (1992).
10. O. M. Efimov, L. B. Glebov, L. N. Glebova, K. C. Richardson, and V. I. Smirnov, ''High-efficiency Bragg gratings in photothermorefractive glass,'' *Appl. Opt.* **38**(4), 619–627 (Feb. 1999).
11. Z. Yaqoob, M. A. Arain, and N. A. Riza, ''High-speed two-dimensional laser scanner by use of Bragg gratings in photothermorefractive glass,'' *Appl. Opt.* **42**(26), 5251–5262 (2003).
12. Z. Yaqoob and N. A. Riza, ''Low loss wavelength-multiplexed optical scanners using volume Bragg gratings for transmit-receive lasercom systems,'' *Proc. SPIE* **5160**, 369–380 (2003).
13. L. D. Dickson, ''Method for making holographic optical elements with high diffraction efficiencies,'' U.S. Patent No. 4,416,505 (1983).
14. H. Kogelnik, ''Coupled wave theory for thick hologram gratings,'' *Bell Syst. Tech. J.* **48**, 2909–2945 (1969).
15. A. Yariv and P. Yeh, *Optical Waves in Crystals: Propagation and Control of Laser Radiation*, John Wiley and Sons, New York (1984).
16. G. Alibert, F. Delorme, P. Boulet, J. Landreau, and H. Nakajima, ''Subnanosecond tunable laser using a single electroabsorption tuning super structure grating,'' *IEEE Photonics Technol. Lett.* **9**(7), 895–897 (1997).
17. Delorme, G. Alibert, C. Ougier, S. Slempkes, and H. Nakajima, ''Sampled-grating DBR lasers with 181 wavelengths over 44 nm and optimized power variation for WDM applications,'' *Opt. Fiber Commun.*, pp. 379–381 (1998).

Nabeel A. Riza graduated from the Illinois Institute of Technology (IIT), Chicago, with highest distinction in 1984 with a BS degree in electrical engineering (EE). He then joined the California Institute of Technology (Caltech) in Pasadena completing his MS degree in 1985, and PhD in 1989, both in EE. Dr. Riza then joined General Electric Corporate Research and Development (GE-CRD) in Schenectady, New York, where he initiated and led the GE Optically Controlled Radar Project. In 1995, he joined the Center for Research and Education in Optics and Lasers (CREOL) at the University of Central Florida (UCF) as an associate professor of EE. As full professor of optics and EE since 2001, Dr. Riza leads the School of Optics/CREOL's first Photonic Information Processing Systems (PIPS) Laboratory which conducts applied optics research in the fields of information optics, defense optics, and heath optics. Dr. Riza's technical contributions described in over 220 publications and 30 patents include works in photonic control systems for phased arrays sensors, liquid crystal devices, fiber optics, biomedical optics, acousto-optic signal processing, optical communications, photonic switching, and interferometry. He received the IIT Alumni Association Academic Achievement Award in 1984, the International Society of Optical Engineering (SPIE) Student Award in 1988, the GE-CRD New Start Award for Innovative Research in 1990, and the GE Gold Patent Medal in 1995. Dr. Riza has served in various capacities for several SPIE and IEEE International Conferences on Photonics. He has also served as an expert panel member for various organizations that include OIDA, NIH, NIST, ONR, NSF, and the Netherlands Scientific Research Organization. From 1996-2001, he served as the Chairman of the IEEE Lasers and Electro-Optics Society (LEOS) Orlando Chapter, and as advisor to the UCF LEOS Student Chapter. Since 2002, he serves as Vice President Memberships for IEEE LEOS. Dr. Riza is the *SPIE Milestone Series* Editor for the Volume 136 "Selected Papers on Photonic Control Systems for Phased Array Antennas" and Co-Editor for the *SPIE Milestone Series* Volume 149 on "Analog Fiber-Optic Links." Dr. Riza is a Senior Member of the IEEE, and received a 1998 Fellow Award of the Optical Society of America (OSA) and a 1998 Fellow Award from SPIE. Dr. Riza is the Winner of the prestigious 2001 International ICO Prize from the International Commission for Optics (ICO) & 2001 Ernst Abbe Medal from the Carl Zeiss Foundation, Germany. To commercialize his inventions, Dr. Riza founded Nuonics, Inc., a small business in Orlando, Florida.

Zahid Yaqoob: Biography and photograph not available.